energies

MDPI

Article

Heavy Oil Laminar Flow in Corrugated Ducts: A Numerical Study Using the Galerkin-Based Integral Method

Valdecir Alves dos Santos Júnior [1,*], Severino Rodrigues de Farias Neto [2], Antonio Gilson Barbosa de Lima [3], Igor Fernandes Gomes [4], Israel Buriti Galvão [5], Célia Maria Rufino Franco [6] and João Evangelista Franco do Carmo [7]

1 Department of Physics and Civil Engineering, Center of Science, Technology and Health, State University of Paraíba, Cel. Pedro Targino Ave, 58233-000 Araruna-PB, Brazil
2 Department of Chemical Engineering, Center of Science and Technology, Federal University of Campina Grande, 882 Aprígio Veloso St, 58428-830 Campina Grande-PB, Brazil; severino.rodrigues@eq.ufcg.edu.br
3 Department of Mechanical Engineering, Center of Science and Technology, Federal University of Campina Grande, 882 Aprígio Veloso St, 58428-830 Campina Grande-PB, Brazil; antonio.gilson@ufcg.edu.br
4 Department of Civil Engineering, Technology Center, Federal University of Pernambuco, Acadêmico Hélio Ramos St, 50670-420 Recife-PE, Brazil; gomes@ufpe.br
5 Department of Mathematics, Center of Science and Technology, State University of Paraíba, 351 Baraúnas St, 58429-500 Campina Grande-PB, Brazil; galvao.mat@gmail.com
6 Department of Physics and Mathematics, Federal University of Campina Grande, 58175-000 Cuité-PB, Brazil; celiarufino@ufcg.edu.br
7 Department of Mechanical Engineering, Federal University of Campina Grande, 58429-900 Campina Grande-PB, Brazil; jevan.franco@gmail.com
* Correspondence: asjrvaldecir@gmail.com; Tel.: +55-83-99961-0088

Received: 20 February 2020; Accepted: 10 March 2020; Published: 15 March 2020

Abstract: Fluid flow in pipes plays an important role in different areas of academia and industry. Due to the importance of this kind of flow, several studies have involved circular cylindrical pipes. This paper aims to study fully developed internal laminar flow through a corrugated cylindrical duct, using the Galerkin-based integral method. As an application, we present a study using heavy oil with a relative density of 0.9648 (14.6 °API) and temperature-dependent viscosities ranging from 1715 to 13000 cP. Results for different fluid dynamics parameters, such as the Fanning friction factor, Reynolds number, shear stress, and pressure gradient, are presented and analyzed based on the corrugation number established for each section and aspect ratio of the pipe.

Keywords: fully developed flow; Galerkin-based integral (GBI) method; Poiseuille number; pressure gradient; petroleum

1. Introduction

The oil industry is a major player in the energy sector worldwide. The increased demand for light oil reserves in recent decades has led to their depletion. As a result, heavy oil is increasingly a topic of interest, receiving considerable attention regarding its efficient transportation. Although there is a large amount of productive crude oil reserves, heavy oil transportation is a complex and expensive task due to its high viscosity, which requires a large amount of energy to pump [1].

One of the major concerns in the production and transportation of heavy oil is related to load loss or pressure drops, which are associated with high flow costs. This occurs due to the fluid friction effect on the inner walls of the duct, making its transport difficult, and increasing the refining cost [2].

Currently, different methods are employed to transport heavy oil from the production field to refineries and markets. Although many other options are available, pipelines are the safest, most efficient, and financially viable means of transporting heavy oil [3].

For many years, analytical and numerical solutions applied to fluid flow inside ducts with arbitrary cross-sections have been studied. Aparecido and Cotta [4] applied generalized integral transform techniques to find solutions for forced laminar convection in rectangular ducts. The same authors, in 1991, presented a generalized integral transform technique for forced laminar convection solutions at the thermal entrance region of ducts with arbitrary cross-sections. Syrjala [5] performed a numerical study related to the laminar flow behavior of viscoelastic fluids in rectangular ducts using the finite element method. Aparecido and Lindquist [6] analytically studied a Newtonian fluid over laminar flow, developed hydrodynamically and thermally, by using generalized integral transformation techniques, with axial and uniform heat flow in straight rectangular ducts. Lee and Kuo [7] applied the Galerkin-based integral method to calculate the Nusselt number for laminar flow in elliptical ducts imposed on the constant duct wall temperature. Values for the coefficient of friction were also found for elliptical ducts with and without a central circular core.

How much to transport of heavy oils, several techniques are employed. These include heat addition, light oil dilution, emulsion formation, and lubrication of the pipe walls with a lower viscosity fluid, all with the aim to reduce the pressure drop along the duct. For transporting a 17.6 Pa·s viscosity oil with a density of 963 kg/m^3 at room temperature using the core-flow technique, Prada and Bannwart [8] found a reduction in the total pressure gradient between 45 and 150 times, compared to that obtained when the oil seeped alone into the pipe. Bensakhria et al. [9] experimentally evaluated the transport of heavy oil with a viscosity of 4.74 Pa·s at a constant temperature of 19.7 °C. The authors observed a reduction in pressure, with a drop of over 90% compared to that obtained with the same oil flowing without parietal lubrication, i.e., without applying the core-flow technique. These authors also observed that the difference in density between water and oil plays an important role in the flow behavior.

Thus, both numerical and experimental simulations are increasingly used to investigate in detail the local dynamics of fluid flow in pipelines, and in particular the importance of transporting heavy oil in this type of modal.

Given the real importance of this problem, in this paper, we propose to carry out a study on the fully developed laminar flow of heavy oil in corrugated cross-section ducts, presenting results for fluid dynamic parameters such as the Poiseuille number, Fanning friction factor, velocity, pressure gradient, shear stress, and Reynolds number, from the solution of the dimensionless momentum equation given by the Galerkin-based integral method, and considering temperature-dependent viscosity. When considering corrugated geometry, there are few works found in the literature. Among these few works, we can cite Casarella et al. [10], Hu and Chang [11], Moharana and Khandekar [12], and Shah [13]. Unfortunately, no work is applied to the petroleum industry.

The motivation for this research is related to the scarcity of work considering this geometry. Among these few works, we have the work of Hu and Chang [11] as a starting point. This work analyzes the fully developed flow over corrugated sine ducts. These authors employed the conformal mapping method and Green's functions to determine fRe and Nu_{H1}. Different from the work of Hu and Chang, where the perimeter is calculated numerically, our work finds the perimeter by the arc length function. This function gives us an exact numeric value of the perimeter. Hu and Chang [11] also applied a perturbation method, the Galerkin internal variational method, and an integral contour equation method to analyze the same problem for corrugated ducts. They found that the perturbation method produced good results for minor disturbances. When the disturbance was large, the results were useful only for qualitative trends. In our research, we use serial approximations of the parameterization of the curve that represents the cross-section of the pipe, because such approximation results in computational gains.

Further, the Galerkin-based integral method has been successfully applied in algorithms in the fields of differential equations [12–14], analysis [15], mechanics, thermodynamics and hydrodynamics [16–19], and also in other engineering fields [20,21]. Specifically, in the calculation of the temperature and/or velocity in ducts, we can cite works with circular, rectangular, isosceles triangular, right triangular, and annuli cross-sections [22–24].

2. Mathematical Formulation

In this work, we choose the cylindrical coordinate system $(r,\ \theta,\ z)$ for the mathematical formulation of the physical problem, and the following assumptions are considered:

(a) The laminar flow is fully developed, isothermal, single-phase, and steady-state;
(b) The cross-sectional area of the tube, along the z-axis, is constant;
(c) The properties of the fluid, thermal and physical, are considered constant;
(d) There is a condition of not-slipping on the duct wall.

2.1. The Geometry

The geometry to be analyzed is a corrugated cylindrical duct. For a duct with corrugated geometry we consider, in polar coordinates, the parameterization of the cross-section, $r(\theta) = a + b\ sin(N\ \theta)$, where a and b are shown in Figure 1 and N is the number of corrugations, sine-type. The relationship $\frac{a}{b}$ is the so-called aspect ratio,

(**a**) (**b**)

Figure 1. (**a**) Aspect ratio in a corrugated duct; (**b**) sine-type corrugated duct.

Thus, considering the cross-section of the duct with the parameterization as reported before, the cross-sectional area of the duct is given as follows:

$$A_c = \frac{1}{2}\int_0^{2\pi} [a + b\ \sin(N\theta)]d\theta, \tag{1}$$

For the perimeter of the cross-section of the duct, we use the definition of arc length as follows:

$$P = \int_0^{2\pi} \sqrt{[a + bsin(N\theta)]^2 + \left[\frac{d}{d\theta}[a + bsin(N\theta)]\right]^2}\, d\theta \tag{2}$$

2.2. Momentum Equation

The momentum equation for the domain and assumptions considered in a cylindrical coordinate system are given by:

$$\frac{\partial^2 u}{\partial r^2} + \frac{1}{r}\frac{\partial u}{\partial r} + \frac{1}{r^2}\frac{\partial^2 u}{\partial \theta^2} = \frac{1}{\mu}\frac{dp}{dz} \tag{3}$$

In the equation, $u(r,\ \theta)$ is the velocity component along the z-axis and annulled in the boundary, μ is the dynamic velocity of the fluid, and $\frac{dp}{dz}$ is the pressure gradient.

By considering the dimensionless variables

$$R = \frac{r}{L} \tag{4}$$

and

$$W(R,\ \theta) = -\frac{u(R,\ \theta)}{\frac{L^2}{\mu}\frac{dp}{dz}} \tag{5}$$

where $L = a$ is the characteristic length, we can write Equation (3) in the dimensionless form and apply it to the hydrodynamically fully developed flow as follows:

$$\frac{\partial^2 W}{\partial R^2} + \frac{1}{R}\frac{\partial W}{\partial R} + \frac{1}{R^2}\frac{\partial^2 W}{\partial \theta^2} = 1,\ \ W = 0 \text{ in } \Gamma \tag{6}$$

The normalized dimensionless mean velocity of the fluid can be obtained as follows:

$$U = \frac{u}{u_m} = \frac{W}{W_m} \tag{7}$$

where u_m and W_m are the mean and dimensionless mean velocity, respectively.

2.3. Solution Methodology

In this work, we have employed the Galerkin-based integral (GBI) method on the MAPLE 17 platform for finding the numerical solution of Equation (6). The solution is approximated as a linear combination of a set of base functions. Thus, for Equation (6), we can write:

$$W = \sum_{i=1}^{n} d_i f_i(R,\ \theta) \tag{8}$$

The bases functions $f_1,\ f_2, \ldots,\ f_n$ are linearly independent functions and satisfy the same homogeneous boundary conditions of W.

Using Equation (8) and applying the GBI method in Equation (6), we obtain the following matrix system:

$$AD = B \tag{9}$$

with

$$a_{ij} = \frac{1}{A_c}\int_{A_c}\left(\frac{\partial^2 f_i}{\partial R^2} + \frac{1}{R}\frac{\partial f_i}{\partial R} + \frac{1}{R^2}\frac{\partial^2 f_i}{\partial \theta^2}\right) f_j dA_c \tag{10}$$

and

$$b_i = -\frac{1}{A_c}\int_{A_c} f_i dA_c \tag{11}$$

The coefficients $d_1,\ d_2, \ldots,\ d_n$ can be determined as follows:

$$D = A^{-1}B \tag{12}$$

In this way, the mean velocity is given by:

$$W_m = \frac{1}{A_c}\int_{A_c} W dA_c = \sum_{j=1}^{n} d_j \frac{1}{A_c}\int_{A_c} f_j dA_c = -\sum_{j=1}^{n} d_j b_j \tag{13}$$

One of the flow parameters commonly used in practice is the Fanning friction factor, f, defined by:

$$f = \frac{\tau_w}{\rho \frac{u_m^2}{2}} \tag{14}$$

where $\tau_w = \frac{d_h}{4}\frac{dp}{dz}$ represents the shear stress and $d_h = \frac{4A_c}{P}$ the hydraulic diameter.

The Reynolds number is defined as:

$$Re = \frac{\rho d_h u_m}{\mu} \tag{15}$$

With these results, we can determine values for the Poiseuille number, which is defined as the product of the Reynolds number and the friction factor as follows:

$$fRe = -\frac{D_h^2}{2W_m} \tag{16}$$

with $D_h = \frac{d_h}{L}$ as the dimensionless hydraulic diameter.

Considering the following parameterization in polar coordinates

$$g(r,\ \theta) = a + b\sin(N\theta) - r, \quad \text{with aspect ratio } \beta = \frac{b}{a} \tag{17}$$

and the set of bases functions of the form,

$$\{f_i\} = \left\{g(r,\ \theta),\ g(r,\ \theta)r^2,\ g(r,\ \theta)\theta^2,\ g(r,\ \theta)r^2\theta^2, \ldots, g(r,\ \theta)r^n\theta^m\right\} \tag{18}$$

we can write the base functions as follows:

$$f_i(r,\theta) = g(r,\ \theta)r^n\theta^m \text{ with } n,\ m = 0,\ 2,\ 4, \ldots,\ N \tag{19}$$

where the subscript i represents the i-th term of the set of base functions in Equation (18).

2.4. Heavy Oil Flow Application

The oil is classified as heavy with °API = 14.6, a relative density of 0.9648 (20/4 °C), and the oil viscosity is reported in Table 1. Thus, we have the value for the fluid density ρ = 952.17 kg/m^3. The cross-section of the duct does not change along the longitudinal direction (z-axis), and we consider an oil mean velocity of u_m = 1 m/s.

Table 1. Values for temperature-dependent kinematic viscosity.

Oil	
T °C	**ν (cS)**
29.22	180.21
51.16	70.786
81.11	25.526
108.5	11.840
137.9	6.3270
155.5	4.4980
199.6	2.3870
228.5	1.6520
260.3	1.1560

3. Results and Discussion

In this section, first, we present the numerical results for the Poiseuille number fRe obtained for the different aspect ratio, β, and the number of corrugations, N, of the corrugated cross-section duct. The effect of the number of corrugations in the shape of the pipe can be observed in Figure 2.

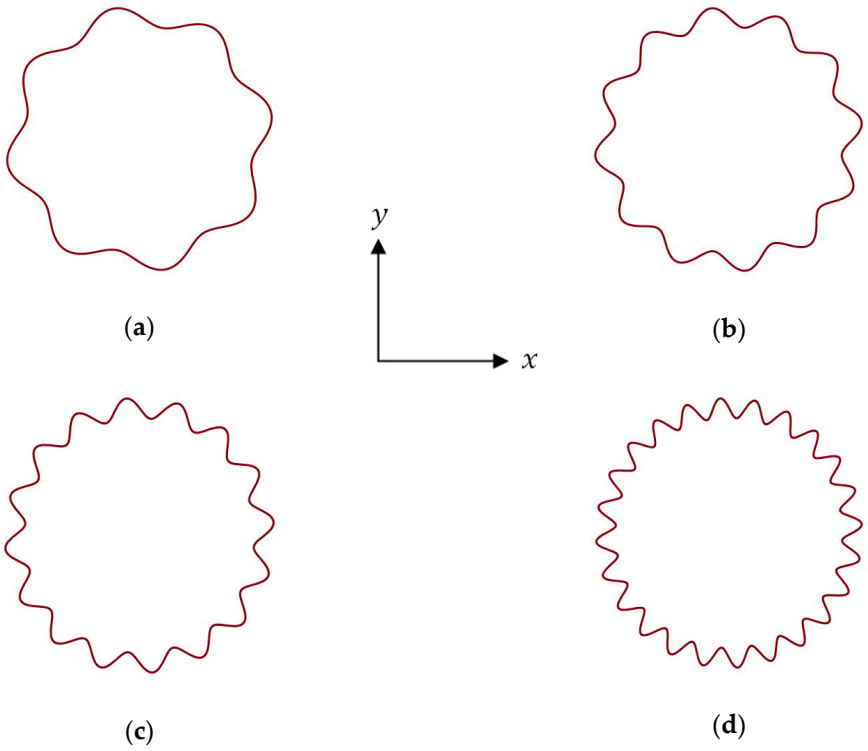

Figure 2. Cross sections of the duct for different numbers of corrugations: (**a**) $N = 8$; (**b**) $N = 12$; (**c**) $N = 16$; (**d**) $N = 24$.

To obtain computational gains, a series approximation is performed for the function that represents the parameterization of the duct cross-section. For example, with $\frac{b}{a} = 0.08$ and $N = 12$, the following approximation can be used:

$$\begin{aligned} 1 + 0.08\ \sin(12\theta) \cong 1 + 0.96\ \theta + \quad & 0.4943780926 \times 10^{-4}\theta^{37} - 0.4572997356 \times 10^{-3}\theta^{35} \\ & + 0.3779074204 \times 10^{-2}\theta^{33} - 0.2771321083 \times 10^{-1}\theta^{31} \\ & + 0.1789811533\ \theta^{29} - 1.009254837\theta^{27} \\ & + 4.920117328\ \theta^{25} - 20.50048887\theta^{23} + 72.03644005\theta^{21} \\ & - 210.1062835\ \theta^{19} + 499.0024232\theta^{17} - 942.5601328\ \theta^{15} \\ & + 1374.566860\theta^{13} - 1489.114099\ \theta^{11} + 1137.517714\ \theta^{9} \\ & - 568.7588571\ \theta^{7} + 165.88 - 23.04\ \theta^{3} \\ & + 2.445874662 \times 10^{-9}\theta^{45} - 1.629074706 \times 10^{-10}\theta^{47} \\ & - 4.80367377 \times 10^{-6}\theta^{39} + 4.217859899 \times 10^{-7}\theta^{41} \\ & - 3.36307766 \times 10^{-8}\theta^{43} \end{aligned} \tag{20}$$

where θ is in radian.

However, no changes are made to the area values and perimeter of the duct. This approximation can be given at least in the first quadrant, because there is a periodicity in this type of geometry. The approximation reported in the series (Equation (20)) can be seen in Figure 3.

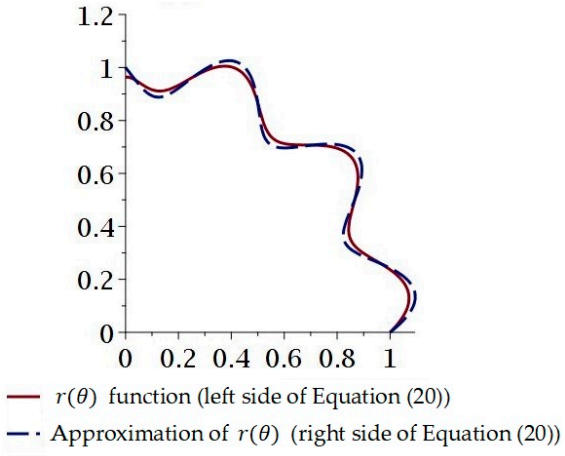

Figure 3. Approximation in series of the function $r(\theta)$.

The fRe values for different cases are presented in Table 2 and compared with the values reported in the literature [13]. Hu and Chang [11] employed the conformal mapping method and Green's functions. It is also important to note that unlike the literature, which uses numerical approximations for the perimeter value, in our work we use the arc length function. The good choice of the parameterization and the number of base functions created a good agreement between the predicted values for this research and the results reported in the literature. In some cases, the choice of the number of base functions from 3 to 52, as can be seen in Table 3, produces a significant increase in the computational time. The minimum computational time for some values was on average 1 minute, while the average maximum time was 2 hours and 15 minutes. Further, it is also observed that the numerical solution with the GBI method is in good agreement with the values reported in the literature. When the aspect ratio value tends to zero, this approximates the predicted Poiseuille number value for the values fRe = 16 obtained for a circular cross-section pipe, validating the mathematical procedure used in this work.

The solution of Equation (7) makes it possible to find the dimensionless velocity distribution, as illustrated in Figure 4:

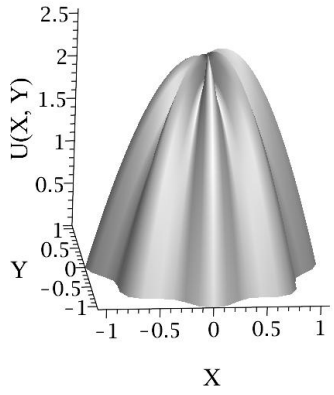

Figure 4. Dimensionless velocity profile (surface curve; $\beta = 0.08$ and $N = 8$).

Note that the graph in Figure 4 is plotted in Cartesian coordinates with $U(X, Y)$, where $X = \frac{x}{L}$ and $Y = \frac{y}{L}$. The values of the parameter fRe for different numbers of corrugations are presented in Table 2 and in Figure 5, for better visualization of this parameter.

In the second part of the results, we present values for the Fanning friction factor, Reynolds number, shear stress, and pressure gradient in corrugated cross-sectional ducts with different aspect ratios changing from β = 0.02 to 0.06, and the number of corrugations N = 8, 12, 16 and 24. In Tables 4–11, these results are shown.

Table 2. Values for Poiseuille number, (fRe), for a different number of corrugations.

N	β	This Work	Ref [13]	N	β	This Work	Ref [13]
8	0.02	16.049	15.990	16	0.02	16.269	15.887
	0.04	16.046	15.962		0.04	15.894	15.542
	0.06	15.918	15.915		0.06	15.015	14.943
	0.08	15.858	15.850		0.08	14.218	14.051
	0.10	15.741	15.765				
	0.12	15.579	15.678				
12	0.02	16.029	15.952	24	0.02	16.043	15.679
	0.04	15.860	15.806		0.04	14.868	14.671
	0.06	15.595	15.559		0.06	12.839	12.872
	0.08	15.216	15.200				
	0.10	14.541	14.711				

Table 3. Values for the number of base functions chosen for each aspect ratio β.

N	β	n	N	β	n
8	0.02	12	16	0.02	12
	0.04	13		0.04	15
	0.06	11		0.06	15
	0.08	7		0.08	5
	0.10	5			
	0.12	5			
12	0.02	30	24	0.02	15
	0.04	52		0.04	15
	0.06	10		0.06	6
	0.08	11			
	0.10	10			

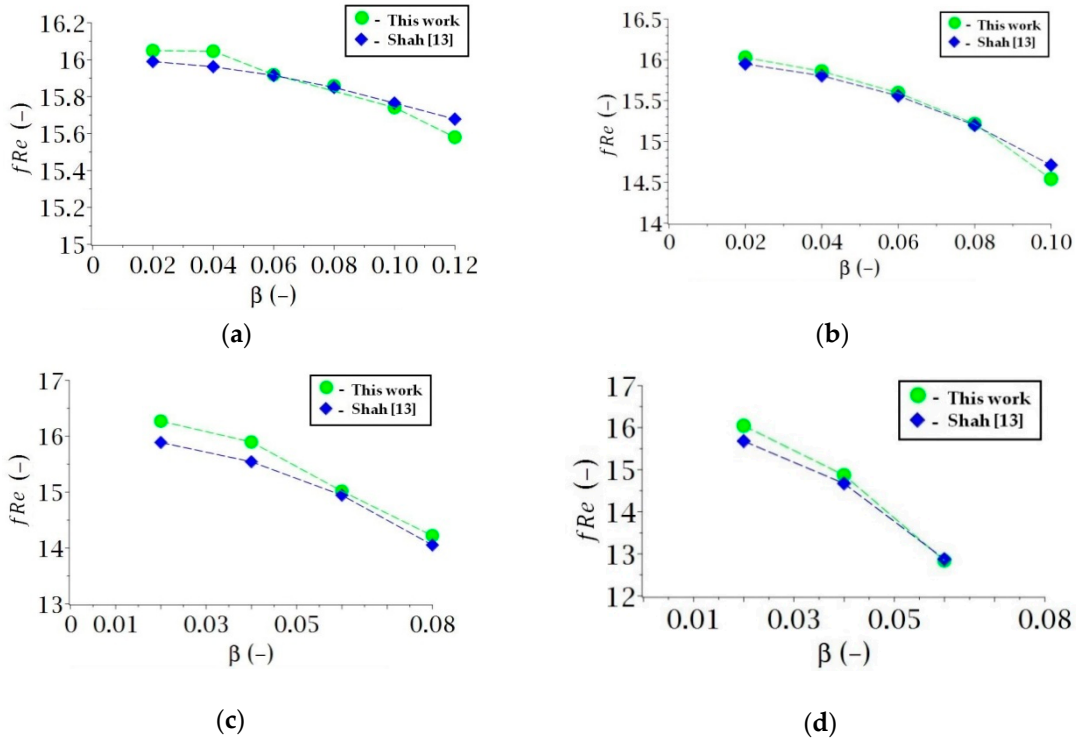

Figure 5. Data of fRe for different aspect ratios (β) of the pipe. (**a**) $N = 8$; (**b**) $N = 12$; (**c**) $N = 16$; (**d**) $N = 24$.

Table 4. Values of the fluid dynamic parameter obtained in the simulations with $\beta = 0.02$ and $N = 8$.

T (°C)	μ (Pa·s)	Re (-)	f (-)	$\bar{\tau}_w$ (Pa)	$\frac{dp}{dz}$ (Pa/m)
29.22	171.60	11.0295	1.4413	686.20	1374.98
51.17	67.400	28.0809	0.5661	269.52	540.061
81.11	24.305	77.8710	0.2041	97.192	194.750
108.5	11.273	167.883	0.0946	45.082	90.3333
137.9	6.0244	314.167	0.0506	24.090	48.2718
155.5	4.2828	441.915	0.0359	17.126	34.3175
199.6	2.2728	832.734	0.0190	9.0887	18.2116
228.5	1.5729	1203.23	0.0132	6.2901	12.6039
260.3	1.1007	1719.49	0.0092	4.4015	8.81970

Table 5. Values of the fluid dynamic parameters obtained in the simulations with $\beta = 0.02$ and $N = 12$.

T (°C)	μ (Pa·s)	Re (-)	f (-)	$\bar{\tau}_w$ (Pa)	$\frac{dp}{dz}$ (Pa/m)
29.22	171.60	10.9438	1.4341	682.77	1404.52
51.16	67.400	27.8627	0.5632	268.17	551.666
81.11	24.305	77.2661	0.2031	96.707	198.935
108.5	11.273	166.579	0.0942	44.856	92.2744
137.9	6.0244	311.726	0.0503	23.970	49.3091
155.5	4.2828	438.482	0.0357	17.041	35.0549
199.6	2.2728	826.265	0.0189	9.0433	18.6029
228.5	1.5729	1193.88	0.0131	6.2587	12.8747
260.3	1.1007	1706.13	0.0091	4.3795	9.00922

Table 6. Values of the fluid dynamic parameters obtained in the simulations with $\beta = 0.02$ and $N = 16$.

T (°C)	μ (Pa·s)	Re (-)	f (-)	$\bar{\tau}_w$ (Pa)	$\frac{dp}{dz}$ (Pa/m)
29.22	29.22	10.82772	1.4482	689.49	1423.29
51.16	51.16	27.56704	0.5688	270.81	559.040
81.11	81.11	76.44601	0.2051	97.658	201.594
108.5	108.5	164.8108	0.0951	45.298	93.5076
137.9	137.9	308.4180	0.0508	24.206	49.9681
155.5	155.5	433.8285	0.0361	17.208	35.5234
199.6	199.6	817.4951	0.0191	9.1323	18.8515
228.5	228.5	1181.211	0.0132	6.3203	13.0468
260.3	260.3	1688.028	0.0092	4.4226	9.12963

Table 7. Values of the fluid dynamic parameters obtained in the simulations with $\beta = 0.02$ and $N = 24$.

T (°C)	μ (Pa·s)	Re (-)	f (-)	$\bar{\tau}_w$ (Pa)	$\frac{dp}{dz}$ (Pa/m)
29.22	171.60	10.51788	1.4104	671.50	1454.98
51.16	67.400	26.77820	0.5539	263.75	571.485
81.11	24.305	74.25849	0.1997	95.110	206.082
108.5	11.273	160.0947	0.0926	44.116	95.5893
137.9	6.0244	299.5925	0.0495	23.574	51.0805
155.5	4.2828	421.4144	0.0352	16.759	36.3142
199.6	2.2728	794.1023	0.0186	8.8940	19.2712
228.5	1.5729	1147.410	0.0129	6.1553	13.3372
260.3	1.1007	1147.410	0.0090	4.3072	9.33287

Table 8. Values of the fluid dynamic parameters obtained in the simulations with $\beta = 0.06$ and $N = 8$.

T (°C)	μ (Pa·s)	Re (-)	f (-)	$\bar{\tau}_w$ (Pa)	$\frac{dp}{dz}$ (Pa/m)
29.22	171.60	10.5343	1.3965	664.89	1391.80
51.16	67.400	26.8200	0.5485	261.15	546.670
81.11	24.305	74.3745	0.1978	94.174	197.133
108.5	11.273	160.344	0.0917	43.682	91.4386
137.9	6.0244	300.060	0.0490	23.342	48.8625
155.5	4.2828	422.072	0.0348	16.594	34.7374
199.6	2.2728	795.342	0.0184	8.8065	18.4344
228.5	1.5729	1149.20	0.0128	6.0948	12.7581
260.3	1.1007	1642.28	0.0089	4.2649	8.92762

Table 9. Values of the fluid dynamic parameters obtained in the simulations with $\beta = 0.06$ and $N = 12$.

T (°C)	μ (Pa·s)	Re (-)	f (-)	$\bar{\tau}_w$ (Pa)	$\frac{dp}{dz}$ (Pa/m)
29.22	171.60	9.93330	1.3399	637.91	1480.35
51.16	67.400	25.2898	0.5262	250.55	581.447
81.11	24.305	70.1312	0.1897	90.353	209.674
108.5	11.273	151.196	0.0880	41.909	97.2556
137.9	6.0244	282.941	0.0470	22.395	51.9710
155.5	4.2828	397.992	0.0334	15.921	36.9473
199.6	2.2728	749.966	0.0177	8.4491	19.6072
228.5	1.5729	1083.63	0.0122	5.8475	13.5697
260.3	1.1007	1548.58	0.0085	4.0918	9.49557

Table 10. Values of the fluid dynamic parameters obtained in the simulations with $\beta = 0.06$ and $N = 16$.

T (°C)	μ (Pa·s)	Re (-)	f (-)	$\bar{\tau}_w$ (Pa)	$\frac{dp}{dz}$ (Pa/m)
29.22	171.60	9.25648	1.2723	605.76	1539.44
51.16	67.400	23.5667	0.4997	237.92	604.658
81.11	24.305	65.3527	0.1802	85.799	218.044
108.5	11.273	140.894	0.0830	39.797	101.138
137.9	6.0244	263.662	0.0440	21.266	54.0456
155.5	4.2828	370.874	0.0310	15.118	38.4222
199.6	2.2728	698.866	0.0168	8.0233	20.3899
228.5	1.5729	1009.80	0.0116	5.5527	14.1114
260.3	1.1007	1443.07	0.0081	3.8856	9.87463

Table 11. Values of the fluid dynamic parameters obtained in the simulations with $\beta = 0.06$ and $N = 24$.

T (°C)	μ (Pa·s)	Re (-)	f (-)	$\bar{\tau}_w$ (Pa)	$\frac{dp}{dz}$ (Pa/m)
29.22	171.60	7.92614	1.1217	534.036	1631.59
51.16	67.400	20.1797	0.4405	209.757	640.854
81.11	24.305	55.9603	0.1588	75.6402	231.097
108.5	11.273	120.645	0.0736	35.0850	107.192
137.9	6.0244	225.769	0.0393	18.7485	57.28089
155.5	4.2828	317.572	0.0279	13.3287	40.7222
199.6	2.2728	598.425	0.0148	7.07330	21.6104
228.5	1.5729	864.674	0.0102	4.89530	14.9562
260.3	1.1007	1235.67	0.0071	3.42553	10.4657

When analyzing the results presented in Tables 4–11, it is observed that the flow of the considered oil has the following behavior: (a) the higher the temperature, the lower the oil viscosity, and (b) the higher the Reynolds number, the lower the friction factor, shear stress, and pressure gradient. The flow remains laminar in all variations of the pipe geometry. Also, when comparing values of the aspect ratio, for example, β = 0.02 and 0.06, and considering the same number of corrugations N, it was observed that the higher the aspect ratio, the greater the pressure gradient. Similarly, if we set a value for the aspect ratio, β, the pressure gradient increases as the number of corrugations N increases. Such statements can be seen in Figure 6.

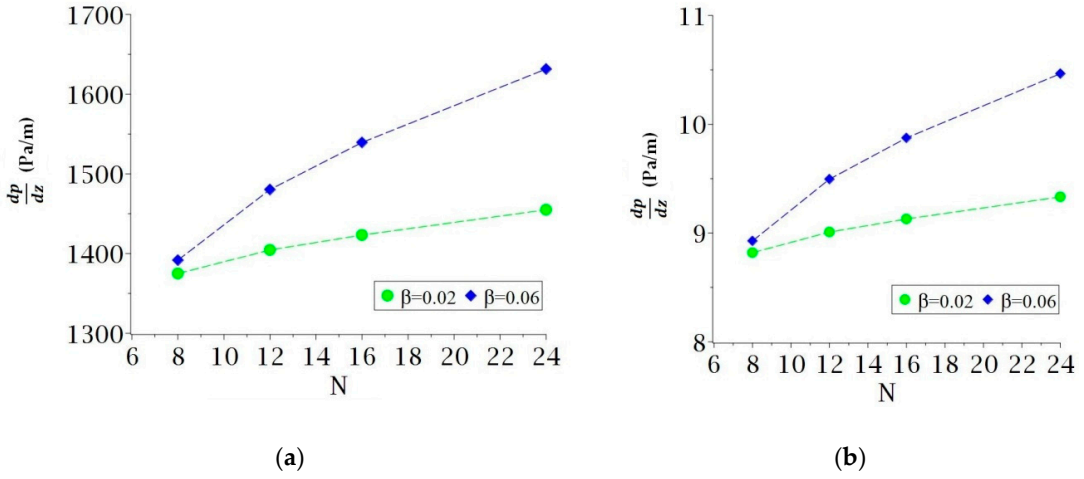

(**a**) (**b**)

Figure 6. The pressure gradient is a function of the number of corrugations for different aspect ratios and fluid temperatures: (**a**) T = 29.22 °C; (**b**) T = 260.3 °C.

4. Conclusions

From the obtained results, the following conclusions can be cited:

1. The Galerkin-based integral method assisted by symbolic manipulation software is an effective tool for investigating the fully developed laminar flow fluid in a corrugated cross-section cylindrical duct. Fully developed velocity profiles for any duct shape can be predicted by this method.
2. The Poiseuille number, fRe, obtained for different aspect ratios of the pipe was compared with the existing literature, and a good concordance was obtained in all studied cases.
3. The appropriate number of base functions is different depending on the aspect ratio and the number of corrugations of the studied geometry. Such variation altered the computational time significantly. The smaller the number of base functions, the lower the computational time.
4. The pressure gradient increases with the number of corrugations and the aspect ratio of the pipe and decreases with the increase in the fluid temperature.
5. Values for the Reynolds number, Fanning friction factor, shear stress, and pressure gradient for heavy oil flow, with temperature-dependent viscosity, were presented. These results make it possible to better understand the behavior of heavy oil in corrugated cross-section ducts.

Author Contributions: Conceptualization, software, and formal analysis, V.A.d.S.J. and S.R.d.F.N.; writing—original draft preparation and editing, V.A.d.S.J.; supervision, review and resources, S.R.d.F.N. and A.G.B.d.L.; validation, formal analysis, review and funding acquisition, I.B.G., I.F.G., C.M.R.F. and J.E.F.d.C. All authors have read and agreed to the published version of the manuscript.

Acknowledgments: The authors thank CNPq, Finep, and Capes (Brazilian Research Agencies) for the financial support, and the authors of the cited references who helped in the improvement.

Conflicts of Interest: The authors declare no conflict of interest.

List of Symbols

a, b	Geometric dimensions (m)
a_{ij}	Element of matrix A
A_c	Cross-section area of the duct (m^2)
A^{-1}	Inverse matrix of A
A, B, D	Matrix
b_j	Element of matrix B (constants)
d_h	Hydraulic diameter (m)
d_j	Constants to be evaluated (constants)
D_h	Dimensionless hydraulic diameter
f	Fanning friction factor (dimensionless)
f_i	Base functions; Galerkin functions
fRe	Poiseuille number (dimensionless)
L	Characteristic length (m)
n	Number of base functions
Nu_{H1}	Nusselt number for the constant flux boundary condition
P	Perimeter (m)
p	Pressure (Pa)
r, θ, z	Cylindrical coordinates
Re	Reynolds number [dimensionless]
u	Local axial velocity (m/s)
T	Temperature (°C)
u_m	Mean velocity (m/s)
U	Normalized velocity (dimensionless)
x, y, z	Cartesian coordinates (m/s)
X, Y, Z	Dimensionless coordinates (dimensionless)
W	Dimensionless velocity (dimensionless)
W_m	Dimensionless mean velocity (dimensionless)
β	Aspect ratio (dimensionless)
μ	Dynamic viscosity (Pa·s)
ν	Kinematic viscosity (cS)
ρ	Density (kg/m^3)
τ_w	Shear stress (Pa)
Γ	Boundary of duct
∇^2	Laplacian operator

Abbreviations

GBI	Galerkin-based integral

References

1. Jadidi, A.; Saleh, S.J. Lubricated Transport of Heavy Oil Investigated by CFD. Ph.D. Thesis, Department of Engineering, University of Leicester, Leicester, UK, 2017.
2. Andrade, T.H.F.; Damacena, Y.T.; Crivelaro, K.C.O.; Farias Neto, S.R.; Lima, A.G.B. *Friction Reduction in Two-Phase Water-Oil Flow in Horizontal Tubes, XV Brazilian Congress of Mechanical Engineering*; Águas de Lindóia: São Paulo, Brazil, 2010. (In Portuguese)
3. Moharana, M.K.; Khandekar, S. Generalized formulation for estimating pressure drop in fully developed laminar flow in singly and doubly connected channels of non-circular cross-sections. *Comput. Methods Appl. Mech. Eng.* **2013**, *259*, 64–76. [CrossRef]
4. Aparecido, J.B.; Cotta, R.M. Thermally developing laminar flow inside rectangular ducts. *Int. J. Heat Mass Transf.* **1990**, *33*, 341–347. [CrossRef]
5. Syrjälä, S. Laminar flow of viscoelastic fluids in rectangular ducts with heat transfer: A finite element analysis. *Int. Commun. Heat Mass Transf.* **1998**, *25*, 191–204. [CrossRef]

6. Aparecido, J.B.; Lindquist, C. *Laminar Forced Convection through Rectangular Ducts with Uniform Axial and Peripheral Heat Flux*; Brazilian Congress of Mechanical Engineering: Águas de Lindóia, Brazil, 1999.
7. Lee, Y.M.; Kuo, Y.M. Laminar flow in annuli ducts with constant wall temperature. *Int. Commun. Heat Mass Transf.* **1998**, *25*, 227–236. [CrossRef]
8. Venegas Prada, J.W. Experimental Study of Annular Oil-Water Flow (Core Flow) in the Elevation of Ultra-Hazardous Oils. Master's Thesis, Petroleum Sciences, and Engineering, State University of Campinas, Campinas, Brazil, 1999. (In Portuguese).
9. Bensakhria, A.; Peysson, Y.; Antonini, G. Experimental study of the pipeline lubrication for heavy oil transport. *Oil Gas Sci. Technol.* **2004**, *59*, 523–533. [CrossRef]
10. Casarella, M.J.; Laura, P.A.; Chi, M. On the approximate solution of flow and heat transfer through non-circular conduits with uniform wall temperature. *Br. J. Appl. Phys.* **1967**, *18*, 1327. [CrossRef]
11. Hu, M.H.; Chang, Y.P. Optimization of finned tubes for heat transfer in laminar flow. *J. Heat Transf.* **1973**, *95*, 332–338. [CrossRef]
12. Shah, R.K. Laminar flow friction and forced convection heat transfer in ducts of arbitrary geometry. *Int. J. Heat Mass Transf.* **1975**, *18*, 849–862. [CrossRef]
13. Courant, R.; David, H. *Methods of Mathematical Physics: Partial Differential Equations*; John Wiley & Sons: New York, NY, USA, 2008.
14. Petrovsky, I.G. *Lectures on Partial Differential Equations*; Dover Publications: New York, NY, USA, 1991.
15. Browder, F.E. *Problemes Non-Lineaires*; Presses de l'Université de Montréal: Montréal, QC, Canada, 1966; Volume 15.
16. Dautray, R.; Lions, J.L. *Mathematical Analysis and Numerical Methods for Science and Technology*; Evolution Problems II; Springer Science & Business Media: Berlin/Heidelberg, Germany, 2012; Volume 6.
17. Assan, A.E. *Finite Elements Methods-First Steps*; Unicamp: Campinas, Brazil, 2003.
18. Cooper, J.M. *Introduction to Partial Differential Equations with MATLAB*; Springer Science & Business Media: Berlin/Heidelberg, Germany, 2012.
19. Thomas, J.E. *Fundamentals of Petroleum Engineering*, 2nd ed.; Interciência, Petrobras: Rio de Janeiro, Brazil, 2004. (In Portuguese)
20. Franco, C.M.R.; Barbosa de Lima, A.G.; Silva, J.V.; Nunes, A.G. Applying liquid diffusion model for continuous drying of rough rice in fixed bed. *Defect Diffus. Forum* **2016**, *369*, 152–156. [CrossRef]
21. Santos, J.P.S.; Santos, I.B.; Pereira, E.M.A.; Silva, J.V.; de Lima, A.G.B. Wheat convective drying: An analytical investigation via galerkin-based integral method. *Defect Diffus. Forum* **2015**, *365*, 82–87. [CrossRef]
22. Haji-Sheikh, A.; Mashena, M.; Haji-Sheikh, M.J. Heat transfer coefficient in ducts with constant wall temperature. *J. Heat Transf.* **1983**, *105*, 878–883. [CrossRef]
23. Lakshminarayanan, R.; Haji-Sheikh, A. Entrance heat transfer in isosceles and right triangular ducts. *J. Thermophys. Heat Transf.* **1992**, *6*, 167–171. [CrossRef]
24. Lee, Y.M.; Lee, P.C. Laminar flow in elliptic ducts with and without central circular cores for constant wall temperature. *Int. Commun. Heat Mass Transf.* **2001**, *28*, 1115–1124. [CrossRef]